A hold-and-feed mechanism drives directional DNA loop extrusion by condensin

Indra A. Shaltiel[1,2], Sumanjit Datta[2,3†], Léa Lecomte[2,3†], Markus Hassler[1,2], Marc Kschonsak[2‡], Sol Bravo[2§], Catherine Stober[2], Sebastian Eustermann[4*], Christian H. Haering[1,2,4*]

[1]Department of Biochemistry and Cell Biology, Julius Maximilian University of Würzburg; 97074 Würzburg, Germany.
[2]Cell Biology and Biophysics Unit, European Molecular Biology Laboratory (EMBL); 69117 Heidelberg, Germany.
[3]Collaboration for joint PhD degree between EMBL and Heidelberg University, Faculty of Biosciences.
[4]Structural and Computational Biology Unit, European Molecular Biology Laboratory (EMBL); 69117 Heidelberg, Germany.
*Corresponding authors. Email: sebastian.eustermann@embl.de, christian.haering@uni-wuerzburg.de
† These authors contributed equally to this work.
‡ Current address: Genentech, South San Francisco, CA.
§ Current address: FeedVax Oral Vaccines, Buenos Aires, Argentina.

Abstract

SMC protein complexes structure genomes by extruding DNA loops, but the molecular mechanism that underlies their activity has remained unknown. We show that the active condensin complex entraps the bases of a DNA loop in two separate chambers. Single-molecule and cryo-electron microscopy provide evidence for a power-stroke movement at the first chamber that feeds DNA into the SMC-kleisin ring upon ATP binding, while the second chamber holds on upstream of the same DNA double helix. Unlocking the strict separation of 'motor' and 'anchor' chambers turns condensin from a one-sided into a bidirectional DNA loop extruder. We conclude that the orientation of two topologically bound DNA segments during the course of the SMC reaction cycle determines the directionality of DNA loop extrusion.

Main text

Members of the SMC (structural maintenance of chromosomes) family of protein complexes have recently emerged as a new class of molecular motors that perform mechanical work on DNA (*1, 2*). In eukaryotes, the cohesin SMC complex delimits large intra-chromosomal loops that are thought to control gene expression during interphase (*3*) and the condensin SMC complex creates arrays of loops that form the structural basis of rod-shaped mitotic chromosomes (*4, 5*). Single-molecule experiments have demonstrated that both complexes can create and processively enlarge DNA loops over tens of kilo-base pairs (kbp) *in vitro* (*6-9*). In these experiments, condensin primarily reeled in DNA from only one side, while cohesin incorporated DNA into the growing loop from both sides.

The molecular mechanism by which these motors couple adenosine triphosphate (ATP) hydrolysis to DNA loop expansion remains unresolved and faces the challenge that it must account for both symmetric and asymmetric loop extrusion by architecturally similar protein complexes. Both complexes are built around a heterodimer of SMC protein subunits that dimerize at a 'hinge' domain located at the end of ~40-nm-long anti-parallel coiled coils (**Fig. 1A**). Sandwiching of two ATP molecules creates a temporary second dimerization interface between 'head' domains at the other end of the coils, which are flexibly connected by a largely unstructured kleisin subunit even in the absence of nucleotide. The central region of the kleisin is bound by two subunits that are composed of consecutive HEAT (Huntingtin, EF3A, PP2A, TOR) repeat motifs (*10, 11*) and have the capacity to interact with DNA and the SMC ATPase heads (*12-18*).

Entrapment of DNA in a confined space is a widespread strategy to achieve processivity of enzymes with dynamic nucleic acid interactions, including DNA polymerase sliding clamps or replicative helicases (*19*), damage repair enzymes MutS (*20*) and Rad50 (*21*), type-II topoisomerases (*22*) or the bacterial motor protein FtsK (*23*). Biochemical and structural evidence support the notion that cohesin (*15-17, 24-26*) and condensin (*27*) topologically constrain DNA, but thus far fell short in revealing whether, and if so how, DNA entrapment can form, let alone enlarge, DNA loops. Here, we

reconstituted the loading of active condensin complexes onto DNA, which enabled us to reconstruct their reaction cycle at molecular detail. We identified chambers within the protein complex that encircle the static and translocating segments of a growing DNA loop and resolved their DNA interactions at near-atomic resolution. Remarkably, disruption of the bicameral separation turns condensin from a strictly unidirectional into a bidirectional DNA loop-extruder. Based on these data, we propose a 'hold-and-feed' reaction cycle that explains directional DNA loop extrusion by SMC protein complexes.

Condensin loads topologically onto DNA without SMC-kleisin ring opening

To define how the condensin complex binds DNA, we developed an *in vitro* system that recapitulates the salt-resistant topological interaction of condensin-chromatin complexes isolated from cells (*27*). We incubated purified *Saccharomyces cerevisiae* (*Sc*) holo condensin with circular plasmid DNA in the presence of ATP and isolated the resulting complexes by immunoprecipitation

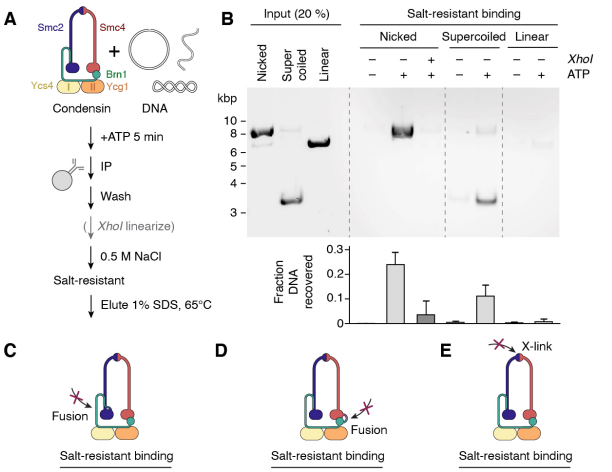

Fig. 1. ATP-dependent topological DNA loading of condensin without SMC-kleisin ring opening. (A) Schematic of the *in-vitro* DNA loading assay. **(B)** Distinct DNA topoisomers bound to condensin after 0.5 M NaCl washing were eluted with 1 % SDS, resolved by agarose gel electrophoresis and quantitated after ethidium bromide staining (mean ± s.d., $n = 4$). **(C)** Condensin with an Smc2−Brn1 fusion was incubated with nicked circular DNA as in (A) and the DNA retained after washing with 0.5 M NaCl quantified in relation to unmodified condensin +ATP (mean ± s.d., $n = 4$). **(D)** Condensin with an Brn1−Smc4 fusion as in (C). **(E)** Unmodified condensin or condensin with a cysteine pair for hinge cross-linking ($Smc2_{K609C}$; $Smc4_{V721C}$) were incubated with dibromobimane (+bBBr) or DMSO solvent prior to addition of nicked circular DNA in the presence of ATP. The amounts of DNA retained after a 0.5 M NaCl wash were quantified as in (C) (mean ± s.d., $n = 3$).

(**Fig. 1A**). A subsequent high-salt wash (0.5 M NaCl) eliminated linear DNA (fig. S1A), which by its nature cannot be topologically confined. Only circular DNA molecules bound in a salt-resistant manner (**Fig. 1B**) and their formation strictly depended on ATP binding and hydrolysis by condensin (fig. S1B). Whereas relaxation of super-helical tension in circular DNA by nicking one strand of the double helix did not affect salt-resistant binding, linearization by endonuclease (*Xho*I) cleavage just prior to or during high-salt washes efficiently released DNA (**Fig. 1B**). We conclude that the interaction between DNA and condensin in the salt-resistant complexes reconstituted from purified components is topological in nature.

The lumen of the Smc2–Smc4–$Brn1^{kleisin}$ ring creates a self-contained space (SMC-kleisin) that seems ideally suited to topologically entrap DNA, which might enter this space upon ATP-dependent dissociation of the Smc2–Brn1 interface (*18*). However, condensin complexes with a covalent peptide fusion of Smc2 to Brn1 (fig. S2A) still formed salt-resistant complexes with circular DNA (**Fig. 1C**), extruded DNA loops with similar efficiency (123/167 DNAs) and rates as their non-fused counterparts (103/127 DNAs) (fig. S3A, movie S1) and supported cell proliferation in *S. cerevisiae* (fig. S4). Similarly, peptide linker fusion of Brn1 to Smc4 (fig. S2B) neither abolished the *in vitro* formation of salt-resistant condensin-DNA complexes (**Fig. 1D**) nor affected DNA loop extrusion efficiencies (176/246 DNAs analyzed) or rates (fig. S3B, movie S1) and supported condensin *in vivo* function (fig. S4). Dibromobimane (bBBr) cross-linking of cysteine residues engineered into the Smc2–Smc4 hinge domains (fig. S2C) did also not impair the formation of salt-resistant DNA complexes (**Fig. 1E**). Titration experiments with mixtures of wild-type and inactive mutant (QL) condensin complexes ruled out that the remaining non-cross-linked complexes were responsible for retaining these DNA molecules (fig. S2D). Together, these results argue against the notion that any of the three subunit interfaces function as a DNA entry gate and call into question whether DNA is at all topologically encircled by the SMC-kleisin ring.

We therefore probed DNA entrapment in the SMC-kleisin ring by analyzing native complexes between condensin and circular mini-chromosomes isolated from yeast cells. We covalently circularized the SMC-kleisin

ring by combining the Smc2–Brn1 fusion with cysteine cross-linking the Smc2–Smc4 and Smc4–Brn1 interfaces (fig. S5). Addition of bBBr simultaneously cross-linked both cysteine pairs in ~20 % of condensin molecules. Yet, unlike for cohesin (*25*), we failed to detect sodium dodecyl sulfate (SDS)-resistant catenanes between the covalently circularized condensin rings and circular mini-chromosomes. Although condensin binds DNA topologically, this topological interaction cannot be explained by a single passage of DNA through the SMC-kleisin ring.

DNA is pseudo-topologically entrapped in two kleisin chambers

Mapping the connectivity of Brn1^{kleisin} segments in structural models of the ATP-free apo state condensin (*28*) indicated the presence of three alternative chambers, each suited to accommodate a DNA double helix (**Fig. 2A**). Chamber I is created by the first ~200 residues of Brn1, which bind the Ycs4^{HEAT-I} subunit and contact the Smc2$_{head}$ region. Chamber II is created by a 'safety belt' loop of ~130 Brn1 residues that forms within the groove of the Ycg1$^{HEAT-II}$ solenoid and has already been shown to entrap DNA (*12*). An intermediate (IA) chamber is created by Brn1 stretches that connect Ycs4 to Ycg1 and Ycg1 to Smc4$_{head}$, respectively. Note that all three kleisin chambers are within the SMC-kleisin tripartite ring circumference and are separated by impermanent protein interfaces: Dissociation of Ycs4 from Smc4$_{head}$ (*18*) fuses chambers I and IA, while disengagement of the 'latch' and 'buckle' segments of the Brn1 safety belt (*12*) fuses chambers IA and II.

We systematically explored the involvement in DNA binding of the three Brn1 chambers and the Smc2–Smc4 lumen by covalent closure of single or combinations of multiple chambers using bBBr cross-linking after condensin had been loaded onto circular DNA *in vitro*. Note that these experiments probed the nucleotide-free apo state of the complex, since ATP supplied for the loading reaction was washed away prior to cross-linking. Closure of Brn1 chamber I (fig. S6A), of chamber II (fig. S6B) or of combined chambers IA and II (fig. S6C) produced SDS-resistant DNA–condensin catenanes that were again resolved by opening with TEV protease cleavage (**Fig. 2B–D**). Similar strategies to circularize chamber IA alone (fig. S6D), the entire Smc2–Smc4–Brn1 ring (fig. S6E) or the Smc2–Smc4 lumen (fig. S6F) failed to produce SDS-resistant catenanes (**Fig. 2E–G**), in contrast to a combination that created a circularized compartment between the Smc2–Smc4 lumen and kleisin chamber I (**Fig. 2H**, fig. S6G).

The only configuration that meets the restraints set by these results (fig. S7) places a DNA loop enclosed simultaneously by chambers I and II into the apo conformation of the complex (**Fig. 2I**). We confirmed that DNA is entrapped in both Brn1 chambers at the same time by opening chambers either individually or in combination with site-specific TEV cleavage (fig. S7A). While opening individual chambers had only minor effects, opening of chambers I or IA in combination with

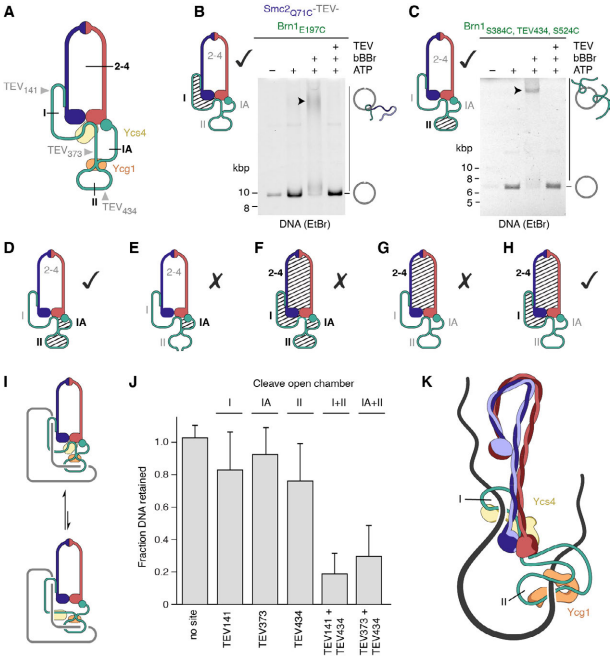

Fig. 2. Condensin constrains DNA in two kleisin chambers. (**A**) Schematic representation of condensin in the ATP-free state. Kleisin chambers I, IA and II and the positions of engineered TEV target sites are indicated. (**B**) Covalent circularization of chamber I (shaded area) by cysteine cross-linking (Smc2$_{Q71C}$; Brn1$_{E197C}$) of the Smc2−Brn1 fusion protein. Agarose gel electrophoresis mobility shift of SDS-resistant condensin-DNA catenanes revealed by ethidium bromide staining. (**C**) Electrophoresis as in (B) after covalent circularization of chamber II (shaded area) by cysteine cross-linking (Brn1$_{S384C, S524C}$). (**D–H**) Additional configurations tested for the formation of SDS-resistant catenanes. Checks and crosses indicate whether catenanes were detected or absent, respectively (fig. S6). (**I**) Schematic configuration of the condensin-DNA complex with equilibrium of chamber I and IA fusion. (**J**) Quantitation of salt-resistant condensin-DNA complexes retained after cleavage at indicated TEV sites within Brn1 (mean ±s.d., $n \geq 3$). (**K**) Model of the DNA path through the ATP-free apo condensin complex.

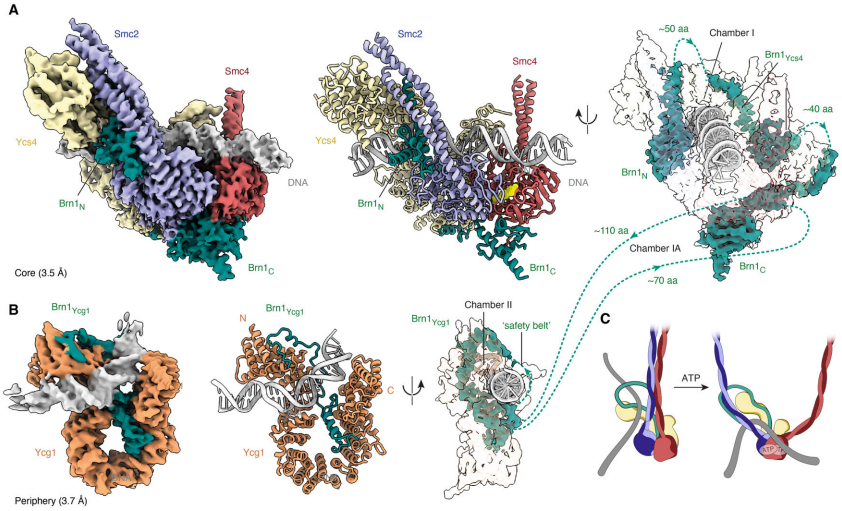

Fig. 3. Cryo-EM structure of ATP-engaged condensin with DNA bound in both kleisin chambers. (**A**) Density map and models of the DNA-bound condensin core subcomplex composed of $Smc2_{head}$ (blue), $Smc4_{head}$ (red), Ycs4 (yellow) and Brn1 (green) resolved to a nominal resolution of 3.5 Å. (**B**) Density maps and models of the DNA-bound condensin peripheral subcomplex composed of Ycg1 (orange) and Brn1 (green) resolved to a nominal resolution of 3.7 Å. Unresolved Brn1 connections are indicated as dotted lines. (**C**) Schematic representation of the tilting motion of DNA entrapped in kleisin chamber I upon ATP binding.

chamber II released the majority of bound DNA (**Fig. 2J**, fig. S8B). Note that the low affinity (K_d = 0.63 µM (*18*)) of the Ycs4–$Smc4_{head}$ interaction that separates chambers I and IA will allow escape of DNA entrapped in chamber I through a gap created in chamber IA during the extended incubation period required for TEV protease cleavage (**Fig. 2I**). The 'pseudo-topological' entrapment of a DNA loop in the SMC-kleisin ring as depicted in **Fig. 2K** explains why none of its interfaces needs to open for DNA entrapment and why ring circularization does not produce denaturation-resistant DNA catenanes – in contrast to cohesin involved in sister chromatid cohesion, which encircles DNA in a truly topological manner (*24, 25*).

Cryo-EM of ATP-bound condensin reveals the role of DNA in kleisin chambers

To gain detailed insight into the fate of bound DNA in kleisin chambers I and II after ATP binding, we trapped a hydrolysis-deficient version (EQ) of the *Sc* condensin holo complex in presence of 50-bp DNA duplexes and determined its structure by cryo-EM. Single-particle analysis revealed a high degree of flexibility among individual molecules. Neural network-based particle picking combined with 3D classification procedures identified two well-ordered yet flexibly linked modules, each bound to a DNA duplex (fig. S9, S10). The quality of cryo-EM reconstructions of each module allowed *de novo* model building for both modules (fig. S11, table S1), facilitated by high-resolution crystal structures of the individual condensin subunits (*12, 18*).

The catalytic 'core' module is composed of $Smc2_{head}$ and $Smc4_{head}$ domains bound to the $Ycs4^{HEAT\text{-}I}$ subunit (**Fig. 3A**), whereas the 'peripheral' module contains the $Ycg1^{HEAT\text{-}II}$ subunit (**Fig. 3B**). Our cryo-EM reconstructions furthermore allowed unambiguous tracing of the $Brn1^{kleisin}$ through the entire complex: Ordered segments of Brn1 ranging from its amino-terminal helix-turn-helix domain ($Brn1_N$) to its carboxy-terminal winged helix domain ($Brn1_C$) thread through both modules. Disordered linker regions connect the segments and consequently flexibly tether the two modules in the DNA-bound state. At both DNA binding sites, the only conceivable paths of the linker regions lead over the bound double helices. Thus, our findings provide a structural basis for understanding the key role of the kleisin subunit for condensin function: Brn1 mediates strategic inter-subunit interactions throughout the complex and simultaneously establishes the formation of two separate, yet flexibly linked chambers that topologically entrap DNA.

A comparison to nucleotide-free apo condensin (*28*) identifies profound conformational rearrangements at the core module, which forms chamber I. Engagement of $Smc2_{head}$ and $Smc4_{head}$ domains by sandwiching ATP at both active sites (fig. S12A) results in a swivel motion, which increases the opening angle between the coiled coils by ~25° to create an open V shape (fig. S12B), resulting in a highly dynamic, opened lumen between the unzipped coils. Ycs4 undergoes a large conformational change (fig. S13), most likely caused by multivalent interactions with $Brn1_N$, the Smc2 coiled coil and approximately half of the 38 visible base pairs of DNA

that are accommodated in the positively charged groove on the concave side of its HEAT-repeat solenoid (fig. S14A). We confirmed the importance of these DNA interactions for *in vivo* condensin function (fig. S14C), DNA-dependent ATPase stimulation (fig. S14D) and DNA loop extrusion (fig. S14E). Homologous DNA interactions are also conserved for cohesin (*15-17*). Although the ATP-free apo structure of condensin adapts a markedly different conformation, most of the local surface of Ycs4 that contacts the DNA backbone remains accessible and unchanged in the absence of nucleotide (fig. S14B), supporting the conclusion that kleisin chamber I also entraps DNA in the ATP-free state.

Taken together, our cryo-EM structures in conjunction with biochemical mapping reveal that the concerted opening the of coiled coils from a tightly zipped (*28*) into an open configuration together with a clamping motion of Ycs4 presumably pushes the DNA in chamber I onto the newly formed binding surface of the engaged $Smc2_{head}$ and $Smc4_{head}$ domains (**Fig. 3C**, fig. S15). This previously unanticipated power-stroke movement elegantly explains how ATP binding might fuel the motor function of condensin by feeding a new DNA loop segment into the inter-coil lumen (see below).

The peripheral module visualizes the structure of kleisin chamber II, which is created by Ycg1 bound to the Brn1 safety-belt segment and flexibly linked to the catalytic 'core'. Whereas a comparison with previous crystal structures shows no major conformational rearrangements of the protein subunits (*12, 29*), the DNA double helix sharply bends almost 90° as it binds to a newly formed composite interface formed by Brn1 and the Ycg1 HEAT-repeat solenoid (fig. S16). This deformation might provide chamber II with the ability to resist longitudinal pulling forces acting on the bound DNA, consistent with a possible anchoring function.

The kleisin chambers provide anchor and motor functions for DNA loop extrusion

Asymmetric DNA loop extrusion by condensin requires that a single complex must grasp both, the immobile ('anchor') and translocating ('motor') DNA segments at the stem of the expanding loop (*6*). If the two identified kleisin chambers were – at least during part of the reaction cycle – responsible for these two functions, release of DNA from the motor chamber should retain condensin on the DNA position where extrusion was initiated. Release of DNA from the anchor chamber should, in contrast, retain condensin at the motor end of the original loop, distal from where loop extrusion started.

We followed the fate of condensin complexes labeled with an ATTO647N fluorophore in single-molecule DNA loop extrusion assays in the presence of TEV protease (**Fig. 4A**). Non-cleavable condensin on DNA loops that ruptured spontaneously was, in most cases (55/59 dissolved loops), retained where loop extrusion had originated and in the remaining few cases (4/59) dissociated upon loop rupture (**Fig. 4B**, fig. S17A, movie S3). We confirmed that condensin remained anchored at its starting position when loops snapped on DNA molecules arched by side-flow (fig. S17B). Spontaneous liberation of condensin-mediated DNA loops thus primarily involves release of DNA from the motor entity,

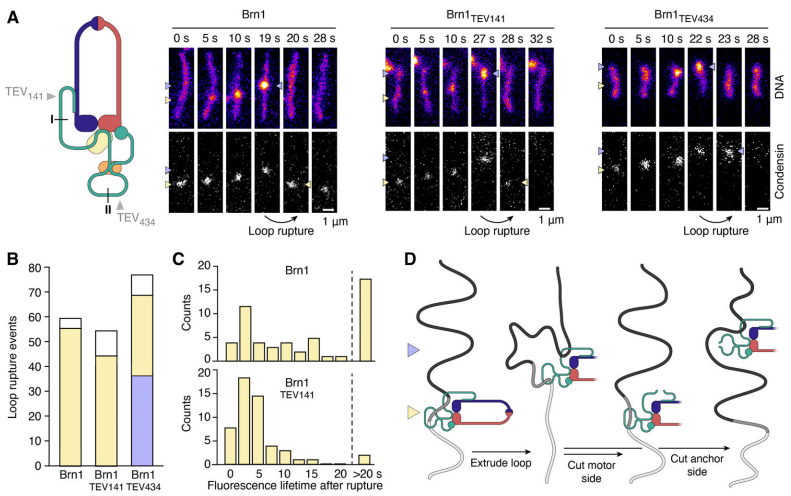

Fig. 4. Identification of motor and anchor chambers. (**A**) Single-molecule DNA loop extrusion on SxO-stained surface-tethered λ-phage DNA (48.5 kbp) molecules by ATTO647N-labeled condensin with TEV cleavage sites introduced in chambers I or II of Brn1. Starting and end positions of the DNA loop are highlighted with yellow and blue arrowheads, respectively. Scale bar = 1 µm. (**B**) The position of condensin 0.5–1 s after DNA loop rupture was scored as non-detectible (white), back at the loop start site (yellow) or on the translocating end of the loop (blue). (**C**) Histogram of ATTO647N-condensin fluorescence lifetimes at the loop start site after loop rupture. (**D**) Schematic representation of experiment and results.

occasionally from both motor and anchor, but never from the anchor entity alone.

DNA loops created by condensin with a TEV cleavage site in chamber I released in a similar manner as spontaneous rupture events (**Fig. 4B**, fig. S17A, movie S4), with condensin retained at the anchor position (44/54) or lost from the DNA (10/54). These events were attributable to opening of chamber I, since we detected the ATTO647N fluorophore attached to $Brn1_N$, which is released from the complex upon TEV cleavage *(18)*, for a considerably shorter time than after spontaneous rupture of non-cleavable condensin (**Fig. 4C**). We conclude that opening of kleisin chamber I releases the motor segment of the DNA loop.

In stark contrast, when loops made by condensin with a TEV cleavage site in kleisin chamber II dissolved, condensin was released from the anchoring position and retained at the translocating site in nearly half of the observed cases (36/76; **Fig. 4B**, fig. S17A, movie S5). In rare instances, condensin continued to translocate in the same direction after loop rupture, now trailing a small DNA density it was no longer able to expand (fig. S17C). We observed several cases of condensin translocation without DNA loop expansion after prolonged incubation with TEV protease (fig. S17D). Consistent with the previous finding that mutation of the kleisin safety belt results in DNA loop slippage *(6)*, our experiments demonstrate that chamber II creates the anchor segment of the DNA loop. The remaining loop rupture events, where condensin remained at the anchor position (32/76) or dissociated (8/76), presumably correspond to spontaneous loop ruptures, which we still expect to occur with TEV-cleavable condensin.

The anchor chamber defines DNA loop extrusion directionality

Our TEV cleavage experiments imply that anchor and motor activities of condensin can be functionally separated. We were able to generate a separation-of-function version for the condensin complex from the filamentous fungus *Chaetomium thermophilum* (*Ct*) (fig. S18A), which displays DNA-stimulated ATPase activity at temperatures up to 50 °C (fig. S18B) and retains much of its affinity for DNA even in the absence of Ycg1, in contrast to *Sc* condensin (fig. S18C).

Ct holo condensin induced local DNA compaction events on tethered DNA molecules (**Fig. 5A**) that emerged as DNA loops upon changing the direction of buffer flow (fig. S19A). DNA loop formation required ATP and Mg^{2+} and was abolished by mutation of the Smc2 and Smc4 ATP-binding sites (QL) (fig. S19B). Remarkably, *Ct* ΔYcg1 condensin initiated the formation DNA loops (**Fig.**

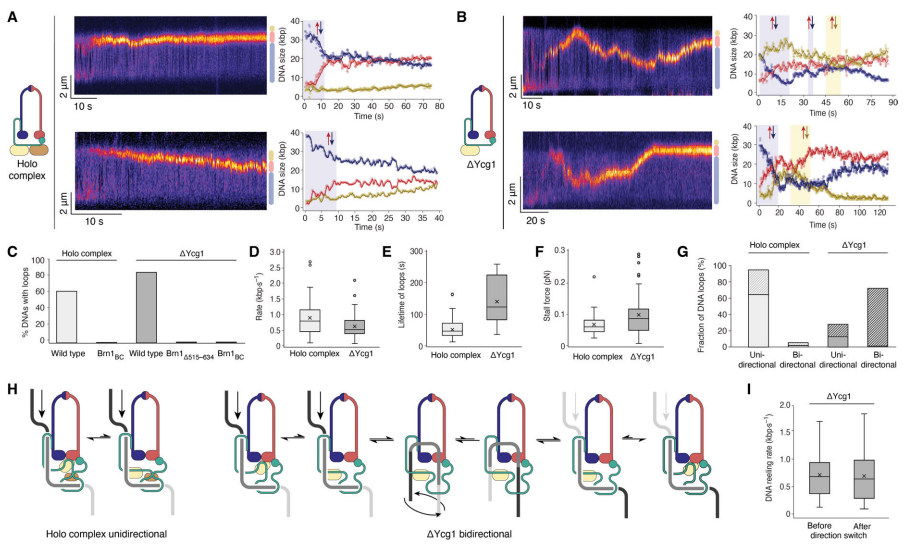

Fig. 5. Merge of DNA chambers enables condensin-mediated DNA loop extrusion to change direction. (**A**) Sample kymographs of DNA loop extrusion by *Ct* holo condensin on λ-phage DNA stained with Sytox orange. Fluorescence intensity plots represent DNA fluorescence above (yellow) or below (blue) the extruded loop (red). (**B**) Sample kymographs of DNA loop extrusion by *Ct* ΔYcg1 condensin as in (A). (**C**) Fraction of DNA molecules displaying loops created by *Ct* holo (wild type or $Brn1_{BC}$) and ΔYcg1 (wild type, $Brn1_{\Delta515–634}$ or $Brn1_{BC}$) condensin (n = 509, 158, 307, 70 or 145 DNAs analyzed). (**D**) Box plot of DNA loop extrusion rates. Lines indicate median, crosses indicate mean, boxes indicate first and third quartile, whiskers mark the median ± 1.5 (third quartile – first quartile). (**E**) Box plot of lifetime of DNA loops as in (D). (**F**) Box plot of stall forces as in (E). (**G**) Fraction of unidirectional or bidirectional DNA loop extrusion events observed for *Ct* holo and ΔYcg1 condensin (n = 56, 79). Shaded areas indicate events that displayed anchor slippage. (**H**) Illustration of a strict separation of motor and anchor DNA segments in holo condensin (left) or exchange of segments in the absence of Ycg1 (right). (**I**) Loop extrusion rates before and after direction switch by *Ct* ΔYcg1 condensin (mean ± s.d., n = 56).

5B) with even greater efficiency than *Ct* holo condensin (**Fig. 5C**). Only when we in addition deleted (Brn1$_{\Delta 515–634}$) or mutated conserved positively charged residues within the Brn1 safety belt loop (Brn1$_{BC}$) did we no longer observe loop extrusion. Quantitation of the DNA loop extrusion parameters revealed that *Ct* ΔYcg1 condensin generated loops at similar rates (**Fig. 5D**). Yet, the lifetime of loops generated by *Ct* ΔYcg1 condensin was significantly increased when compared to loops generated by *Ct* holo condensin (**Fig. 5E**), which otherwise snapped soon after the complex reached the stall force for loop extrusion (**Fig. 5F**). We conclude that kleisin chamber II, but not the presence of Ycg1, is essential for condensin-mediated DNA loop extrusion.

Like condensin from other species (*6, 9*), *Ct* holo condensin almost exclusively reeled in DNA unidirectionally (53/56 DNA loops; **Fig. 5G**, fig. S20A, movie S6). In contrast, *Ct* ΔYcg1 condensin frequently switched directions during loop extrusion (57/79; **Fig. 5G**, fig. S20B, movie S7). On some DNA molecules, the DNA loop changed direction as many as six times within a 120-seconds imaging window (fig. S20B, movie S8). The changes in direction were sometimes difficult to discern when they overlapped with anchor slippage events, which were more frequent for DNA loops generated by *Ct* ΔYcg1 condensin than for holo condensin (**Fig. 5G**), but could clearly be identified in the majority of cases when the loop size further increased as condensin reeled in DNA from the opposite direction (fig. S21A). The change in loop extrusion direction is hence not simple backtracking of condensin's motor entity. It can also not be explained by the action of a second condensin complex that moves into the opposite direction, since such an event would have resulted in the formation of Z-loop structures, which are easily recognizable by the elongated DNA density (*30*) and were rare under the conditions of our assay (fig. S21B).

We propose that the observed turns instead reflect an exchange of motor and anchor DNA segments within the extruding condensin complex (**Fig. 5H**). If this were the case, the speed of loop extrusion should be identical in either direction. Loop extrusion rates after switching direction were indeed very similar to the original translocation rates (**Fig. 5I**).

A hold-and-feed mechanism drives SMC-mediated DNA loop extrusion

SMC complexes stand out from conventional DNA motor proteins by their ability to translocate in steps of kilo-base pairs in length (*6-8*). Current models for the molecular mechanism of DNA loop extrusion fail to explain how consecutive steps can proceed in a directional manner on a DNA substrate that lacks intrinsic polarity (*31*). Biochemical mapping of the path of DNA through two kleisin chambers (**Fig. 2**), structures of the identical protein complex in ATP-free *(28)* and ATP-bound (**Fig. 3**) states and the assignment of motor and anchor functions to the DNA binding sites by single-molecule imaging (**Fig. 4**) now provide the foundation for a mechanistic description of the SMC-mediated DNA loop extrusion cycle:

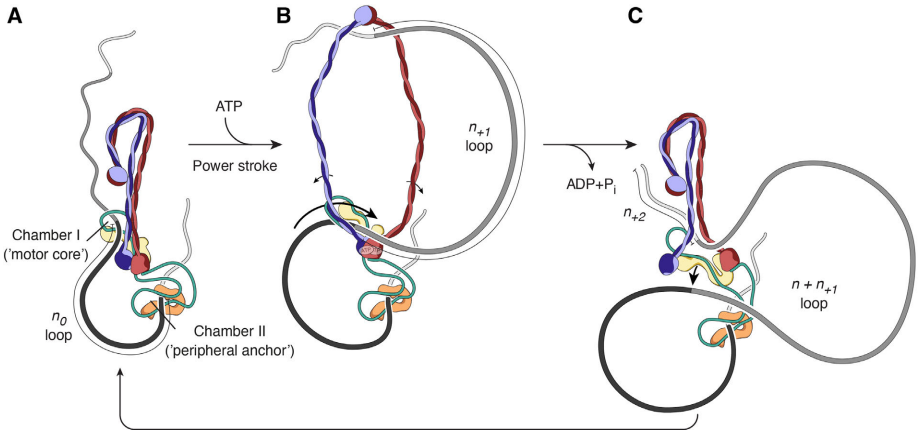

Fig. 6. A hold-and-feed mechanism for SMC-mediated DNA loop extrusion. (**A**) After loading, ATP-free condensin entraps a DNA loop (n_0) pseudo-topologically between kleisin chambers I and II. (**B**) ATP binding drives SMC head dimerization, coiled-coil opening and Ycs4^{HEAT-I} repositioning to feed DNA held in kleisin chamber I in-between the SMC coiled coils at the SMC motor core (power stroke). The result is the pseudo-topological entrapment of a new DNA loop (n_{+1}) in the coiled-coil lumen. (**C**) ATP hydrolysis drives the transition into the ATP-free 'bridged' state of the SMC motor to release one n_{+1} DNA segment, while the peripheral anchor remains bound upstream. This step merges both loops ($n_0 + n_{+1}$). Return to the ground state configuration repositions the remaining n_{+1} DNA segment into chamber I. Condensin is now ready to extrude the next DNA loop (n_{+2}). Fig. S22 summarizes structural information supporting each step as well as possible intermediates of the reaction cycle.

The DNA-segment-capture model (*32*) proposes that SMC dimers grasp DNA loops generated by random thermal motion. Our data instead suggest that the concerted tilting of a DNA double helix that is entrapped in kleisin chamber I actively feeds DNA in-between the unzipped coiled coils upon ATP-mediated SMC head engagement (**Fig. 6A**, fig. S22A). As a result of this power-stroke motion, two DNA loops are now pseudo-topologically entrapped by the condensin complex (**Fig. 6B**). To reset the complex to the apo state following nucleotide hydrolysis, SMC head disengagement most likely first results in the 'bridged' conformation observed previously (*28*). As a consequence, the head-proximal segment of the newly captured loop releases from kleisin chamber I (**Fig. 6C**). Simultaneously, zipping up of the SMC coiled coils (*32, 33*) and/or tilting of the latter onto the folded coils (*28, 34*) move the distal loop segment towards the ATPase heads, where it remains confined between HEAT-repeat subunit I and the SMC coiled coils. To regenerate the initial conformation with DNA in kleisin chamber I, this DNA segment then merely has to tilt into the DNA-binding groove of the HEAT-repeat subunit, which is only possible in one direction due to geometric restrictions.

DNA entrapment in kleisin chamber I hence ensures that translocation proceeds processively and in a single direction, always threading the next DNA segment into the SMC coiled-coil lumen from the same end of the DNA loop. This translocation mechanism explains how condensin can step over flexibly tethered obstacles that are many times its size (*35*), while nevertheless binding DNA pseudo-topologically (fig. S22B).

DNA entrapment in kleisin chamber II is essential for anchoring condensin to DNA (*6, 12*), whereas HEAT-repeat subunit II is not (**Fig. 5**). This finding is inconsistent with a recently proposed Brownian ratchet mechanism as the fundamental principle for DNA loop extrusion by SMC complexes (*36*). The HEAT-repeat subunit is, however, required to close off the kleisin safety belt and thereby separate anchor and motor strands of the DNA loop, since its absence from the condensin complex turns an exclusively unidirectional DNA loop extruder into one that frequently switches direction. The natural merge of chambers II and IA in the absence of a kleisin safety belt in cohesin (*12, 13*) presumably allows for a frequent exchange of motor and anchor strands (*7, 8*), which explains how monomeric cohesin can extrude DNA loops bidirectionally. Binding of the cohesin HEAT-II subunit to the CTCF boundary factor most likely prevents strand exchange and thereby provides a molecular account for the CTCF convergence rule for topologically-associating domains (*37*). Confinement of the DNA in two kleisin chambers thus not only forms the basis of DNA translocation but also dictates the directionality of loop extrusion by SMC protein complexes.

References

1. I. F. Davidson, J. M. Peters, Genome folding through loop extrusion by SMC complexes. *Nat Rev Mol Cell Biol*, (2021).
2. S. Yatskevich, J. Rhodes, K. Nasmyth, Organization of Chromosomal DNA by SMC Complexes. *Annu Rev Genet* **53**, 445-482 (2019).
3. M. S. van Ruiten, B. D. Rowland, On the choreography of genome folding: A grand pas de deux of cohesin and CTCF. *Curr Opin Cell Biol* **70**, 84-90 (2021).
4. T. Hirano, Capturing condensin in chromosomes. *Nat Genet* **49**, 1419-1420 (2017).
5. J. H. Gibcus *et al.*, A pathway for mitotic chromosome formation. *Science* **359**, (2018).
6. M. Ganji *et al.*, Real-time imaging of DNA loop extrusion by condensin. *Science* **360**, 102-105 (2018).
7. I. F. Davidson *et al.*, DNA loop extrusion by human cohesin. *Science* **366**, 1338-1345 (2019).
8. Y. Kim, Z. Shi, H. Zhang, I. J. Finkelstein, H. Yu, Human cohesin compacts DNA by loop extrusion. *Science* **366**, 1345-1349 (2019).
9. S. Golfier, T. Quail, H. Kimura, J. Brugues, Cohesin and condensin extrude DNA loops in a cell cycle-dependent manner. *Elife* **9**, (2020).
10. C. H. Haering, J. Lowe, A. Hochwagen, K. Nasmyth, Molecular architecture of SMC proteins and the yeast cohesin complex. *Mol Cell* **9**, 773-788 (2002).
11. I. Onn, N. Aono, M. Hirano, T. Hirano, Reconstitution and subunit geometry of human condensin complexes. *EMBO J* **26**, 1024-1034 (2007).
12. M. Kschonsak *et al.*, Structural Basis for a Safety-Belt Mechanism That Anchors Condensin to Chromosomes. *Cell* **171**, 588-600 e524 (2017).
13. Y. Li *et al.*, Structural basis for Scc3-dependent cohesin recruitment to chromatin. *Elife* **7**, (2018).
14. I. Piazza *et al.*, Association of condensin with chromosomes depends on DNA binding by its HEAT-repeat subunits. *Nat Struct Mol Biol* **21**, 560-568 (2014).
15. Z. Shi, H. Gao, X. C. Bai, H. Yu, Cryo-EM structure of the human cohesin-NIPBL-DNA complex. *Science* **368**, 1454-1459 (2020).
16. T. L. Higashi *et al.*, A Structure-Based Mechanism for DNA Entry into the Cohesin Ring. *Mol Cell* **79**, 917-933 e919 (2020).
17. J. E. Collier *et al.*, Transport of DNA within cohesin involves clamping on top of engaged heads by Scc2 and entrapment within the ring by Scc3. *Elife* **9**, (2020).

18. M. Hassler *et al.*, Structural Basis of an Asymmetric Condensin ATPase Cycle. *Mol Cell* **74**, 1175-1188 e1179 (2019).

19. T. R. Beattie, S. D. Bell, Molecular machines in archaeal DNA replication. *Curr Opin Chem Biol* **15**, 614-619 (2011).

20. M. H. Lamers *et al.*, The crystal structure of DNA mismatch repair protein MutS binding to a G x T mismatch. *Nature* **407**, 711-717 (2000).

21. L. Kashammer *et al.*, Mechanism of DNA End Sensing and Processing by the Mre11-Rad50 Complex. *Mol Cell* **76**, 382-394 e386 (2019).

22. G. Hauk, J. M. Berger, The role of ATP-dependent machines in regulating genome topology. *Curr Opin Struct Biol* **36**, 85-96 (2016).

23. T. H. Massey, C. P. Mercogliano, J. Yates, D. J. Sherratt, J. Lowe, Double-stranded DNA translocation: structure and mechanism of hexameric FtsK. *Mol Cell* **23**, 457-469 (2006).

24. T. G. Gligoris *et al.*, Closing the cohesin ring: structure and function of its Smc3-kleisin interface. *Science* **346**, 963-967 (2014).

25. C. H. Haering, A. M. Farcas, P. Arumugam, J. Metson, K. Nasmyth, The cohesin ring concatenates sister DNA molecules. *Nature* **454**, 297-301 (2008).

26. M. Srinivasan *et al.*, The Cohesin Ring Uses Its Hinge to Organize DNA Using Non-topological as well as Topological Mechanisms. *Cell* **173**, 1508-1519 e1518 (2018).

27. S. Cuylen, J. Metz, C. H. Haering, Condensin structures chromosomal DNA through topological links. *Nat Struct Mol Biol* **18**, 894-901 (2011).

28. B. G. Lee *et al.*, Cryo-EM structures of holo condensin reveal a subunit flip-flop mechanism. *Nat Struct Mol Biol* **27**, 743-751 (2020).

29. K. Hara *et al.*, Structural basis of HEAT-kleisin interactions in the human condensin I subcomplex. *EMBO Rep* **20**, (2019).

30. E. Kim, J. Kerssemakers, I. A. Shaltiel, C. H. Haering, C. Dekker, DNA-loop extruding condensin complexes can traverse one another. *Nature* **579**, 438-442 (2020).

31. M. Hassler, I. A. Shaltiel, C. H. Haering, Towards a Unified Model of SMC Complex Function. *Curr Biol* **28**, R1266-R1281 (2018).

32. J. F. Marko, P. De Los Rios, A. Barducci, S. Gruber, DNA-segment-capture model for loop extrusion by structural maintenance of chromosome (SMC) protein complexes. *Nucleic Acids Res* **47**, 6956-6972 (2019).

33. M. L. Diebold-Durand *et al.*, Structure of Full-Length SMC and Rearrangements Required for Chromosome Organization. *Mol Cell* **67**, 334-347 e335 (2017).

34. F. Burmann *et al.*, A folded conformation of MukBEF and cohesin. *Nat Struct Mol Biol* **26**, 227-236 (2019).

35. B. Pradhan *et al.*, SMC complexes can traverse physical roadblocks bigger than their ring size. *bioRxiv*, 2021.2007.2015.452501 (2021).

36. T. L. Higashi, G. Pobegalov, M. Tang, M. I. Molodtsov, F. Uhlmann, A Brownian ratchet model for DNA loop extrusion by the cohesin complex. *Elife* **10**, (2021).

37. Y. Li *et al.*, The structural basis for cohesin-CTCF-anchored loops. *Nature* **578**, 472-476 (2020).

38. T. Terakawa *et al.*, The condensin complex is a mechanochemical motor that translocates along DNA. *Science* **358**, 672-676 (2017).

39. D. J. Fitzgerald *et al.*, Protein complex expression by using multigene baculoviral vectors. *Nat Methods* **3**, 1021-1032 (2006).

40. J. Schindelin *et al.*, Fiji: an open-source platform for biological-image analysis. *Nat Methods* **9**, 676-682 (2012).

41. M. Schorb, I. Haberbosch, W. J. H. Hagen, Y. Schwab, D. N. Mastronarde, Software tools for automated transmission electron microscopy. *Nat Methods* **16**, 471-477 (2019).

42. J. Zivanov *et al.*, New tools for automated high-resolution cryo-EM structure determination in RELION-3. *Elife* **7**, (2018).

43. A. Punjani, J. L. Rubinstein, D. J. Fleet, M. A. Brubaker, cryoSPARC: algorithms for rapid unsupervised cryo-EM structure determination. *Nat Methods* **14**, 290-296 (2017).

44. S. Q. Zheng *et al.*, MotionCor2: anisotropic correction of beam-induced motion for improved cryo-electron microscopy. *Nat Methods* **14**, 331-332 (2017).

45. A. Rohou, N. Grigorieff, CTFFIND4: Fast and accurate defocus estimation from electron micrographs. *J Struct Biol* **192**, 216-221 (2015).

46. D. Tegunov, P. Cramer, Real-time cryo-electron microscopy data preprocessing with Warp. *Nat Methods* **16**, 1146-1152 (2019).

47. T. Bepler *et al.*, Positive-unlabeled convolutional neural networks for particle picking in cryo-electron micrographs. *Nat Methods* **16**, 1153-1160 (2019).

48. P. B. Rosenthal, R. Henderson, Optimal determination of particle orientation, absolute hand, and contrast loss in single-particle electron cryomicroscopy. *J Mol Biol* **333**, 721-745 (2003).

49. E. F. Pettersen *et al.*, UCSF ChimeraX: Structure visualization for researchers, educators, and developers. *Protein Sci* **30**, 70-82 (2021).

50. P. Emsley, B. Lohkamp, W. G. Scott, K. Cowtan, Features and development of Coot. *Acta Crystallogr D Biol Crystallogr* **66**, 486-501 (2010).

51. J. Jumper *et al.*, Highly accurate protein structure prediction with AlphaFold. *Nature* **596**, 583-589 (2021).

52. T. I. Croll, ISOLDE: a physically realistic environment for model building into low-resolution electron-density maps. *Acta Crystallogr D Struct Biol* **74**, 519-530 (2018).

53. P. V. Afonine *et al.*, Real-space refinement in PHENIX for cryo-EM and crystallography. *Acta Crystallogr D Struct Biol* **74**, 531-544 (2018).

54. J. F. Marko, E. D. Siggia, Statistical mechanics of supercoiled DNA. *Phys Rev E Stat Phys Plasmas Fluids Relat Interdiscip Topics* **52**, 2912-2938 (1995).

Acknowledgments

We thank Jenny Ormanns and Jutta Metz for assistance with the generation of yeast strains, Shveta Bisht for protein purification, Fabian Merkel for advice and help with cryo-EM, Robin Stipp for help setting up insect cell expression, Thomas Hoffmann for scientific computing support, Marko Lampe of the EMBL Advanced Light Microscopy Facility, Felix Weis of the EMBL Cryo-Electron Microscopy Platform and the Proteomics Core Facilities.

Funding

European Research Council grant 681365 (CHH), Dutch Research Council Rubicon grant 019.2015.1.310.025 (IAS), Jeff-Schell Darwin Trust PhD Studentship (SD)

Author contributions

IAS, SD, MK and SB purified condensin complexes; IAS performed *in vitro* DNA loading assays; IAS and SD performed single-molecule experiments; LL and SE performed cryo-EM experiments and processed data; LL, SE and MH built structure models; IAS and CS performed yeast experiments; SE and CHH supervised the work and acquired funding; IAS, SE and CHH wrote the manuscript with input from all authors.

Competing interests

Authors declare that they have no competing interests.

Data and materials availability

All data are available in the main text or the supplementary materials. Plasmids, yeast strains and image analysis scripts will be made available upon request. Coordinates of DNA-bound condensin are available in pdb under accession numbers xxx (core) and xxx (periphery).

Supplementary Materials

Materials and Methods
Figs. S1 – S22
Tables S1 – S2
Movies S1 – S8